Energy and Buildings 42 (2010) 1779–1789

Contents lists available at ScienceDirect

Energy and Buildings

journal homepage: www.elsevier.com/locate/enbuild

Modeling of energy performance of a house with three configurations of building-integrated photovoltaic/thermal systems

S. Pantic*, L. Candanedo, A.K. Athienitis

Department of Building, Civil and Environmental Engineering, Concordia University, 1515 St. Catherine West, Montreal, Quebec, Canada, H3G 2W1

ARTICLE INFO

Article history:
Received 16 February 2009
Received in revised form 28 February 2010
Accepted 15 May 2010

Keywords:
Building-integrated photovoltaic/thermal system
Thermal storage
Energy performance

ABSTRACT

A theoretical and experimental study of energy performance of three different open loop air heating building-integrated photovoltaic/thermal (BIPV/T) systems that utilize recovered heat for home heating is presented. The configurations are: Configuration 1: base case of unglazed BIPV with airflow under it; Configuration 2: addition of 1.5 m vertical glazed solar air collector in series with Configuration 1; Configuration 3: addition of a glazing over the PV. The model developed has been verified against experimental data from a solar research house for Configuration 1. Obtained relationships for BIPV/T system exiting air temperature as function of solar irradiance and air speed in PV cavity may be used for developing fan airflow control strategies to achieve desired outlet air temperature suitable for different applications. For Configuration 1, preheated air is suitable for HVAC system and domestic hot water (DHW) preheating. Higher outlet air temperatures of the PV cavity suitable for DHW might be achieved by utilizing Configurations 2 or 3. With Configuration 2, significant outlet air temperatures are achieved in winter along with enhanced thermal efficiency making it suitable for coupling with a rockbed heat storage. Finally, Configuration 3 significantly reduces electricity production and may lead to excessively high PV panel temperatures.

1. Introduction

Photovoltaic panels integrated into a building envelope are a promising technology in sustainable building design. They can replace conventional building elements such as roof shingles while generating heat and power simultaneously. When both electricity and useful heat is generated from a building-integrated photovoltaic (BIPV) system it is defined as a BIPV/thermal or BIPV/T system (or PV/T if it is a modular system). BIPV/T systems can be open loop—usually with outdoor air as the cooling fluid or closed loop with water (or some other fluid) as the cooling fluid flowing through attached piping similar to solar collectors. BIPV/T systems can reduce building energy consumption [1] and total installation cost of PV systems, reducing payback time. Simple payback time of roof and façade PV/T systems linked to HVAC system for industrial and residential applications have been evaluated by Bazilian at al. [2] who suggested that BIPV/T systems are suitable for low temperature space and water heating. Various researchers have studied energy performance of PV panels integrated into façades Correlations for convective heat transfer coefficients in photovoltaic/thermal systems have been developed [3]. A theoretical study of ventilated double-facades with integrated PV investigated the effect of different design parameters on thermo-electrical performance of the system [4]. Simulation studies of different types of PV collector integration into tilted roof and vertical façade have been carried out by Guiavarch and Peuportier [5] and annual generated electricity, recovered heat and overall efficiency have been determined with respect to PV technology, climate and thermal interaction between the PV collector and building. Others focused on closed water loop solar systems linked to HVAC system; simulation results of wall-mounted water type PV/T collector connected to a water tank indicated an optimum water mass flow rate and solar cell packing factor in the system for achieving desired energy output [6]. Finally, Bakker et al. [7] studied roof-integrated uncovered PV/T panels coupled with a ground source heat pump and concluded that the concept could meet space heating load, DHW demands and almost all electrical load.

However, little research has been done on quantifying the relative energy performance of open loop air-based BIPV/T roof linked to HVAC systems. This paper presents a simulation and experimental study of energy performance of three different open air loop BIPV/T roof systems coupled with different heat recovery and thermal storage systems: air-water heat exchanger to heat DHW, water storage tank and rockbed. The three BIPV/T roof configurations are as follows: Configuration 1: a base case of PV with airflow under it; Configuration 2: addition of a vertical glazed collector section

* Corresponding author. Tel.: +1 514 848 2424; fax: +1 514 848 7965.
E-mail address: usrobotics011@yahoo.com (S. Pantic).

0378-7788/$ – see front matter © 2010 Elsevier B.V. All rights reserved.
doi:10.1016/j.enbuild.2010.05.014

Nomenclature

A_i	area of surface i (m^2)
ACH	air changes per hour
AHU	air handling unit
AWHE	air-water heat exchanger
BIPV/T	building-integrated photovoltaic/thermal system
CHTC	convective heat transfer coefficients
$c_{p,i}$	specific heat capacity of i (J/kgK)
C_i	thermal capacitance of i (J/K)
$\dot{C}_i$	heat capacity rate of i (W/K)
DHW	domestic hot water
E_r	heat storage capacity (Wh)
h_i	convective heat transfer coefficient of i (W/m^2K)
H_i	height of i (m)
I	current (A)
k_i	thermal conductivity of i (W/K)
m	number of PV panels
m_i	mass of i (kg)
$\dot{m}_i$	mass flow rate of i (kg/s)
n	days of heat storage
P	perimeter (m)
P_{el}	generated electricity (W)
Pr	Prandtl's number
q	internal heat source (W)
Q	exchanged heat (W)
r	rockbed
R_i	thermal resistance of i (m^2K/W)
Ra	Rayleigh's number
Re	Reynolds' number
S	total incident solar radiation (W/m^2)
SAC	solar air collector
Δt	time step (min)
T_i	temperature of element i (K)
U_i	thermal conductance of i (W/K)
V	voltage (V)
V_i	velocity of i (m/s)
Vol_i	volume of i (m^3)
y, z, L	length (m)
W	width (m)

Subscripts

abs	absorber
c	cold fluid
e	exterior
h	hot fluid
HE	heat exchanger
i	interior
o	outdoor
oc	open circuit
pv	photovoltaic
rad	radiative
ref	reference
sc	short circuit
w	water

Greek

α_{pv}	absorptivity of PV panel (assumed 0.9)
β	tilt angle (°)
εi	surface emissivity of i
η_i	efficiency of i
ρ_i	density of i (kg/m^3)
τ_i	transmittance of i
σ	Stefan–Boltzmann constant = 5.67×10^{-8} ($W/m^2\,K^4$)

Fig. 1. Photo of Concordia solar house.

to Configuration 1 to increase outlet air temperature; Configuration 3: addition of a glazing over the PV. Concordia solar house [8], depicted in Fig. 1, has been used as a case-study to verify the developed model for Configuration 1. The solar house was originally built as Canada's entry for the Solar Decathlon Competition 2005 held in Washington D.C., USA [9]. Thus, the roof layout was designed to maximize the capture of solar energy in Washington D.C. limiting the height and roof slopes of solar house. Since then, it was modified and converted into a research facility at Concordia University. In addition, a demonstration solar house was designed and built with similar BIPV/T system to that of the Concordia solar house by collaborating with a prefabricated home builder [10].

2. Model development

2.1. Introduction

Building designers are faced with many challenges in solar housing design. Integration of PV panels into buildings is more than simply connecting electrical and building envelope components. The PV panels should be integrated appropriately to maximize the use of solar energy and increase cost effectiveness. Some of the major questions to be considered in BIPV/T system design are how much electricity can be generated, how much heat can be recovered and how to use it and what type of BIPV/T roof configuration will yield the best performance. For example, by increasing the airflow in the air gap under the PV panels two objectives are achieved: the temperature of the PV panels is lowered, resulting in electrical efficiency increase and air thermal efficiency is enhanced. Higher flow rates result in higher thermal efficiency but the recovered heat may not be useful due to low air temperature at the outlet of the BIPV/T system. One reason that open loop air system (as opposed to closed loop) is attracting attention for heating applications is that it allows keeping PV panel temperature lower than with a closed loop system; a lower PV operating temperature contributes to a longer lifetime for the panels and increase in electricity production. Further, preheated outdoor air can be used in a ventilation system as fresh air or to contribute to space heating. Not only active solar systems but also passive solar systems such thermal mass, properly oriented advanced fenestration, overhangs, motorized blinds may also be used in solar building design. Often solar energy is available but typically not needed for immediate use because passive solar heat gains may satisfy daytime heating loads in cold climates. The excess heat recovered from an open loop BIPV/T air system may be used for different heating purposes such as stored in a thermal storage for later use or used to heat water through air-water heat exchanger or as a source for a heat pump. This paper focuses on utilization of the heat recovered from three BIPV/T system configurations using an HVAC air system, a rockbed and an air-water heat

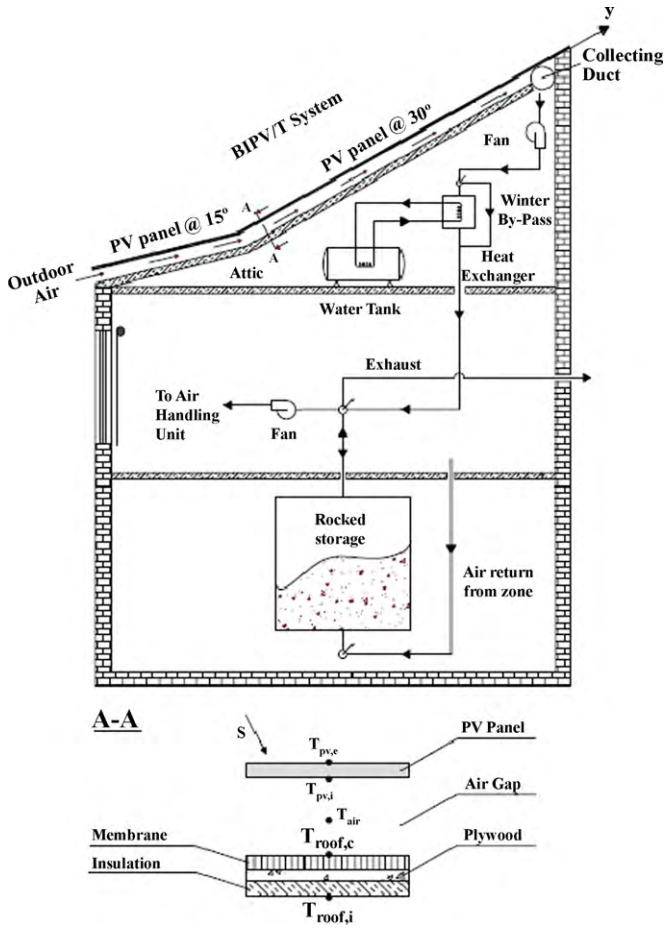

Fig. 2. Configuration 1—unglazed BIPV/T system.

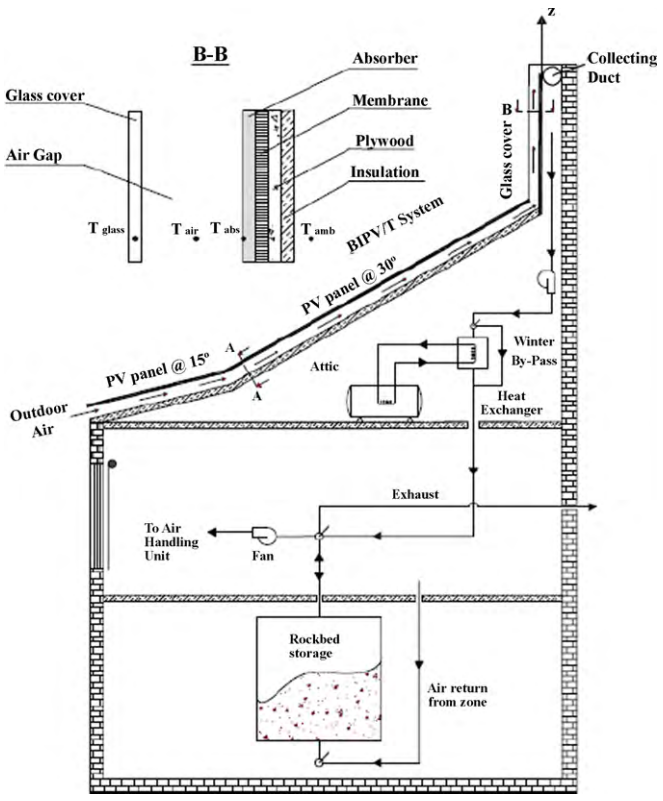

Fig. 3. Configuration 2—unglazed BIPV/T system with SAC.

exchanger linked to a DHW tank. The following section presents the methodology used in this investigation.

Lumped parameter thermal models require the use of convective heat transfer coefficients for the air channel formed by the PV module and the roofing material in order to solve for the temperatures in the thermal network. These coefficients are affected by different factors such as heating asymmetry, air moisture content, mass flow rates and cross section of the PV channel—for example, elements such as the PV framing contribute to increased turbulence; hence, enhancing the convective heat transfer coefficients. This paper uses well known correlations for the convective heat transfer coefficients developed for laminar, transitional and turbulent flow, and for natural convection for the case of an open ended channel.

2.2. System configurations

Three different open air loop BIPV/T system configurations linked to HVAC components have been considered in this study. Configuration 1, a base case of unglazed PV panels with airflow under them, is depicted in Fig. 2. An alternative setup, referred to as Configuration 2 shown in Fig. 3, where 1.5 m long flat plate solar air collector (SAC) is vertically added to Configuration 1 to increase the outlet air temperature of the unglazed BIPV/T system section during winter when the solar altitude is low. Finally, Configuration 3 is shown in Fig. 4 and resembles a flat solar air collector where PV panels are used as absorber plate with a glazing cover. For all configurations, a 7 kW PV system consisting of 40 mono-crystalline BP4175 PV panels integrated into a south-facing roof has been con-

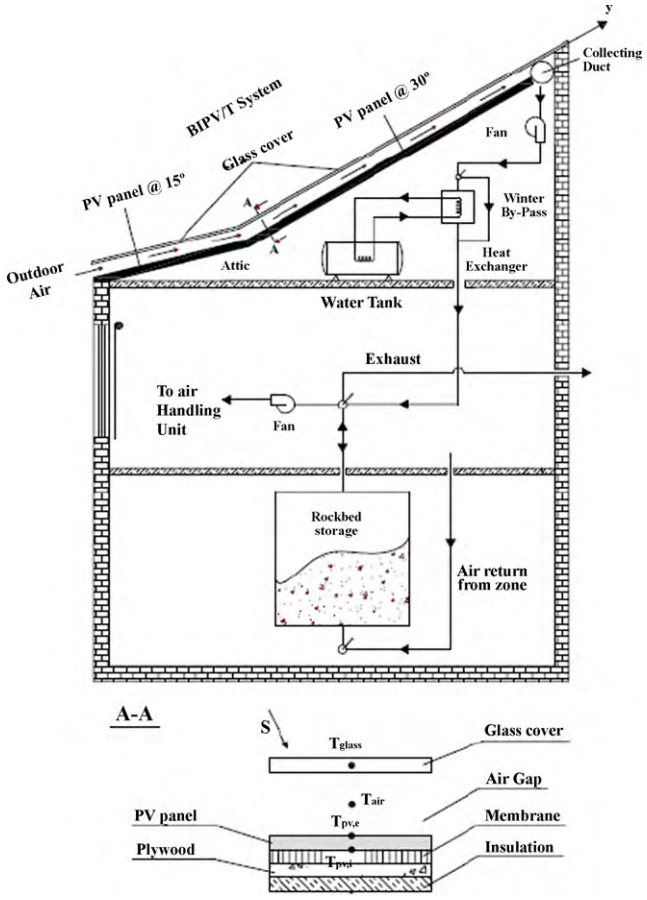

Fig. 4. Configuration 3—glazed BIPV/T system.

sidered with a 4 cm deep air cavity through which ambient air is drawn by a variable speed fan. The roof has two sections—one at slope of 15° connecting to a second section at 30°. The first section, with a 15° slope, measures 9.5 m × 1.6 m and consists of 2 rows with 6 PV panels each. The section with 30° slope has 4 rows with 7 PV panels each and has dimension of 11.1 m × 3.2 m. When immediate space heating is required, outdoor air is heated by recovered heat from the BIPV/T system, supplied to an air handling unit for additional heating or delivered directly into a zone. When solar heat gains through south windows can meet daytime heating load, the recovered heat from the BIPV/T system is stored in the rockbed storage for later use. During cold winter nights, the stored heat is extracted by circulating room air through the rockbed storage. The air-water heat exchanger (AWHE) is by-passed in winter. In summer mode, total airflow through air cavity is circulated through AWHE and exhausted outside. Heated water in AWHE is used to heat water in a water tank for DHW needs.

2.3. BIPV/T model

A mathematical model has been implemented in MathCad 2001i [11] for the three BIPV/T system configurations. The roof has been divided into three sections with lengths of 1.6 m each, one at 15° slope and two at 30° slope as it has been found suitable for adequate degree of accuracy. A control volume formulation has been applied with the outlet air temperature of one section used as input value to the next section. Average temperatures of the control volumes and air of the first section are initially guessed. The initial convective heat transfer coefficients (CHTC) and air properties are calculated based on guessed temperature values and an iterative energy balance procedure is repeated until sufficient convergence has been achieved (less than 0.1 °C difference in temperatures). The same procedure is repeated for the other two sections. Major assumptions used in simulations are: one-dimensional heat transfer, isothermal surfaces of the PV channel for each segment, no air leakage in the PV cavity, uniform solar radiation incident on clean and exterior surfaces and air stream temperature varies linearly along the BIPV/T system for short lengths, CHTC values for upper and lower surface of the PV cavity are equal and PV modules operate at their maximum power point condition.

Based on reviewed PV models available in various building energy simulation programs, Motilo et al. [12] recommend a modified one-diode equivalent PV model. The new one-diode model takes into account temperature dependence of short-circuit current and open-circuit voltage utilizing empirical coefficients commonly provided by manufacturers. The short-circuit current, open-circuit voltage and maximum PV power output are be obtained from Eqs. (1)–(3) [12]:

$$I_{sc} = I_{sc,ref}\frac{\tau^*_{glass}\cdot S}{S_{ref}}[1+\alpha(T_{pv}-25\,^\circ\mathrm{C})] \tag{1}$$

$$V_{oc} = V_{oc,ref}[1-\gamma(T_{pv}-25\,^\circ\mathrm{C})\cdot \max\left(1+\beta\ln\left(\frac{\tau^*_{glass}\cdot S}{S_{ref}}\right)\right) \tag{2}$$

$$P_{el} = I_{mp,ref}\cdot V_{mp,ref}\left(\frac{I_{sc}\cdot V_{oc}}{I_{sc,ref}\cdot V_{oc,ref}}\right)\cdot m \tag{3}$$

where * refers to Configuration 3, S_{ref} = 1000 W/m^2 is irradiance at standard test conditions, α (1/°C) is temperature coefficient of I_{sc}, β (1/°C) is temperature coefficient of V_{oc} and γ is dimensionless irradiance coefficient of V_{oc}.

For the case of unglazed BIPV/T system, Configuration 1 depicted in Fig. 2, the corresponding energy balance Eqs. (4)–(7) are as follows:

PV node-exterior

$$U_o\cdot(T_{pv,e}-T_o)+U_{pv}\cdot(T_{pv,e}-T_{pv,i})+P_{el}=\alpha_{pv}\cdot S\cdot A_{pv} \tag{4}$$

PV node-interior

$$U_{pv}\cdot(T_{pv,i}-T_{pv,e})+U_{h_1}\cdot(T_{pv,i}-T_{air})=U_{rad}\cdot(T_{roof,e}-T_{pv,i}) \tag{5}$$

Roof node-exterior

$$U_{rad}\cdot(T_{roof,e}-T_{pv,i})+U_{h2}\cdot(T_{roof,e}-T_{air}) = U_{roof}\cdot(T_{roof,i}-T_{roof,e}) \tag{6}$$

Roof node-interior

$$U_{roof}\cdot(T_{roof,i}-T_{roof,e})=U_{attic}\cdot(T_{attic}-T_{roof,i}) \tag{7}$$

Previous studies have demonstrated that temperature profile in the ventilated cavity should be exponential [4]. In the model, change in enthalpy of air in the control volume is equal to the energy transferred to the air by convection. The energy balance on the air is as follows:

$$W\cdot h_1(T_{pv,i}-T_{air})+W\cdot h_2(T_{roof,e}-T_{air})=\dot{m}_{air}\cdot c_{p,air}\cdot\frac{dT_{air}}{dy} \tag{8}$$

Solution of Eq. (8) is given by Eq. (9):

$$T_{air}(y) = \exp\left[-\frac{(h_1+h_2)\cdot W\cdot y}{m_{air}\cdot c_{p,air}}\right]\cdot T_{in} + \left[1-\exp\left(-\frac{(h_1+h_2)\cdot W\cdot y}{m_{air}\cdot c_{p,air}}\right)\right]\cdot \times\left(\frac{h_1\cdot T_{pv,i}+h_2\cdot T_{roof,e}}{h_1+h_2}\right) \tag{9}$$

where T_{in} is the inlet air temperature. In the case of first section, T_{in} equals ambient temperature. For subsequent BIPV/T system sections, outlet air temperature of previous section has been used as an input value to the next section. The mean air temperature is obtained by integrating T_{air} from y = 0 to L with boundary condition that inlet air temperature is equal to the ambient temperature.

$$\overline{T_{air}} = \frac{1}{L}\int_0^L T_{air}(y)dy \tag{10}$$

For the case of BIPV/T-SAC system, Configuration 2 depicted in Fig. 3, Eqs. (11)–(13) have been employed to calculate node temperatures by using the same algorithm described previously. A 1.5 m long SAC is linked vertically to the unglazed BIPV/T section to increase air outlet temperature. The channel depth has been set to 4 cm. The optical properties of glazing cover as a function of angle of incidence, glass thickness, refractive index and extinction coefficient have been calculated [13]. Absorber values for conductivity (k_{sac}) of 0.04 W/m K, thickness (x_{sac}) of 0.025 m and absorptance (α_{abs}) of 0.95 have been assumed.

Glass covernode

$$(T_{glass}-T_o)\cdot U_o+(T_{glass}-T_{air})\cdot U_{h_1} +(T_{glass}-T_{abs,e})\cdot U_{rad}=\alpha_{glass}\cdot S\cdot A_{sac} \tag{11}$$

Absorber node

$$(T_{abs,e}-T_{glass})\cdot U_{rad}+(T_{abs,e}-T_{air})\cdot U_{h_i} +(T_{abs,e}-T_{abs,i})\cdot U_{abs}=\tau_{glass}\cdot\alpha_{abs}\cdot S\cdot A_{sac} \tag{12}$$

Energy balance of the air

$$W\cdot h_1(T_{glass}-T_{air})+W\cdot h_2(T_{abs,e}-T_{air})=\dot{m}_{air}c_{p,air}\frac{dT_{air}}{dz} \tag{13}$$

Glazed BIPV/T system (Configuration 3 shown in Fig. 4) has been modeled according to Eqs. (11)–(13) where PV panels have been used as absorbers (with an additional term in the energy balance corresponding to electricity produced). Collected heat (Q_{heat}), heat losses (Q_{loss}), reflected solar radiation (S_{refl}) and generated electricity (P_{el}) can be expressed with Eqs. (14)–(19):

$$Q_{heat} = \dot{m}_{air} \cdot c_{p,air} \cdot (T_{air,out} - T_o) \quad (14)$$

$$Q_{loss,top} = U_o \cdot (T_{pv,e} - T_o) \quad (15)$$

$$Q^*_{loss,top} = U_o \cdot (T_{glass,e} - T_o) \quad (16)$$

$$Q_{loss,bottom} = U_{roof} \cdot (T_{roof,e} - T_{roof,i}) \quad (17)$$

$$Q^*_{loss,bottom} = U_{pv} \cdot (T_{pv,e} - T_{pv,i}) \quad (18)$$

$$S_{refl} = (1 - \alpha_{pv}) \cdot A_{pv} \cdot S \cdot \tau^*_{glass} \quad (19)$$

With these definitions, energy balance for unglazed and glazed BIPV/T system can be written as:

$$A_{pv} \cdot S = Q_{heat} + Q_{loss,top} + Q_{loss,bottom} + P_{el} + S_{refl} \quad (20)$$

In order to compare thermal performance of the systems with thermodynamic optimum, heat removal factor (F_R) has been calculated as follows [13]:

$$F_R = \frac{\dot{m}_{air} \cdot c_{p,air}}{A_{pv} \cdot U_L} \left[1 - e^{-\left(\frac{A_{pv} U_L F'}{\dot{m}_{air} c_{p,air}} \right)} \right] \quad (21)$$

where efficiency factor (F') has been determined as:

$$F' = \frac{h_1 h_r + h_2 U_o + h_2 h_r + h_1 h_2}{(U_o + h_r + h_1) \cdot (U_{pv} + h_2 + h_r) - h_r^2} \quad (22)$$

$$U_L = \frac{(U_{pv} + U_o) \cdot (h_1 h_2 + h_1 h_r + h_2 h_r) + U_{pv} U_o (h_1 + h_2)}{h_1 h_r + h_2 U_o + h_2 h_r + h_1 h_2} \quad (23)$$

where h_r (W/m^2 K) represents radiation heat transfer coefficient given by Eq. (24):

$$h_r = \frac{4 \cdot \sigma \cdot \left(T_1^2 + T_2^2 \right) \cdot (T_1 + T_2)}{1/\varepsilon_1 + 1/\varepsilon_2 - 1} \quad (24)$$

2.4. Convective heat transfer coefficients

Many correlations have been developed to determine convective heat transfer coefficients in a channel. These correlations are valid for different situations depending on nature of the flow. The flow can be driven by forced, natural or mixed convection. It can be either laminar or turbulent and for the entrance region might be in the developing flow stage [4]. The flow can be approximated as flowing in a circular duct using hydraulic diameter concept, in a rectangular channel and between parallel plates. In this investigation, it has been assumed that flow may start as laminar in the inlet section due to smooth entrance and no abrupt change in the direction. It has been assumed that both temperature and velocity profiles develop simultaneously in the entry region due to absence of an unheated starting length. Laminar flow in the entrance region for developing and fully developed flow when Re < 2300, has been described by Eq. (25) [14]:

$$h_c = \frac{k_{air}}{D_h} \left[1.86 \cdot \left(\frac{RePrD_h}{L} \right)^{1/3} \cdot \left(\frac{\mu}{\mu_s} \right)^{0.14} \right] \quad (25)$$

where dynamic viscosity (μ/μ_s) was calculated for the air mean/surface temperature, respectively. The equation is valid for constant surface temperature T_s, $0.48 < Pr < 16700$ and $0.0044 < (\mu/\mu_s) < 9.75$. Furthermore, the equation is recommended for the values of $(RePrD_h/L)^{1/3} \cdot (\mu/\mu_s)^{0.14} \geq 2$. For fully developed flow, the convective coefficient is calculated as follows:

$$h_c = \frac{7.54 \cdot k_{air}}{D_h} \quad (26)$$

For transition flow region, Eq. (27) has been employed [15]:

$$h_c = \frac{k_{air}}{D_h} \left[0.116 \cdot (Re^{2/3} - 125) \cdot Pr^{1/3} \cdot \left(1 + \left(\frac{D_h}{L} \right)^{2/3} \right) \cdot \left(\frac{\mu}{\mu_s} \right)^{0.14} \right] \quad (27)$$

The above correlation is valid for $2300 < Re < 6000$. For turbulent flow region where $6000 < Re < 10^6$, the correlation below [16] has been used:

$$h_c = \frac{k_{air}}{D_h} \left[\frac{\left(\frac{f}{8} \cdot (Re - 1000) \cdot Pr \right)}{1 + 12.7 \cdot \sqrt{\frac{f}{8}} \cdot (Pr^{2/3} - 1)} \cdot \left(1 + \left(\frac{D_h}{L} \right)^{2/3} \right) \right] \quad (28)$$

where friction factor f is calculated as follows:

$f = (1.82 \log Re - 1.64)^{-2}$. The equation is valid for $0 < D_h/L < 1$ and $0.6 < Pr < 2000$.

The above equations have been used for forced flow. Hydraulic diameter (D_h) has been calculated as twice the separation distance between the plates. Outdoor CHTC have been calculated as the sum of convective and radiation part. DOE-2 outdoor convection model with respect of wind speed, surface roughness and orientation has been applied in the model [17]. Radiation heat exchange between exterior surfaces, sky and ground has been linearized for simplicity.

2.5. Building model

A mathematical model describing thermal response of the solar house with unglazed PV panels integrated into roof has been implemented in MathCad 2001i software. The 75 m^2 house has been modeled as a single zone.The thermal network model approach has been used to simulate transient thermal behaviour of the house and the thermal network equations are solved by explicit finite difference method as follows [18]:

$$T(i, t+1) = \left(\frac{\Delta t}{C_i} \right) \left[q_i + \sum_j \frac{T(j,t) - T(i,t)}{R(i,j)} \right] + T(i,t) \quad (29)$$

where C_i represents the thermal capacitance attached to node i, $R(i,j)$ it thermal resistance between nodes i and j and t is the present time step ($t+1$ is the next time step). Indoor CHTC between the room surfaces and indoor air applied in [18] have been used. Radiation heat transfer between all interior surfaces has been modeled using view factors. Incident solar radiation on a surface has been calculated using Hottel's model for the clear sky [18]. Solar radiation and outdoor temperatures were modeled by discrete Fourier series. In order to simplify calculations, it has been assumed that 70% of transmitted solar radiation through double glazed low-e windows has been absorbed by the floor and the rest by other surfaces. Ground temperature has been assumed to be equal to that of ambient temperature. BLAST design sky model has been used for estimating the sky temperature [17]. Internal heat gains from lights, people and appliances were also modeled on hourly basis. Infiltration has been determined for the ventilated attic and zone by Eq. (30):

$$U_{inf} = \frac{ACH \cdot Vol_z}{3600} \cdot \rho_{air} \cdot c_{p,air} \quad (30)$$

Infiltration of 0.5 air changes per hour (ACH) has been assumed. Room set point temperature of 22 °C has been assumed. A simulation time step of 5 min has been chosen for calculations as it was found suitable for adequate degree of desired accuracy.

2.6. Air to water heat exchanger model

An unmixed counter-flow fluid heat exchanger with constant heat effectiveness has been modeled [14]. The maximum possible sensible heat transfer has been based on a minimum capacity rate of fluids entering the AWHE.

2.7. Water tank model

A mathematical model of a cylindrical horizontal water tank with a heating coil developed by [13] has been used for analysis. It has been assumed that there were no heat losses from pipe connections of the AWHE to a water tank and to surroundings. Thermal non-stratified water tank has been assumed. The thermal energy balance for a 151 l water tank with RSI 2.5 installed at the solar house is described by Eq. (31):

$$m_w \cdot c_{pw} \cdot \frac{dT_w(t)}{dt} = Q_{HE}(t) - U_{tank}\,[T_w(t) - T_o(t)] \quad (31)$$

Eq. (33) can be solved under reasonable assumption that exchanged heat in the AWHE Q_{HE} (t) is constant over the small time step, e.g. 5 min. A more accurate model for the tank can be developed by considering about five control volumes [13].

2.8. Thermal rockbed storage model

A mathematical model of vertical thermal rockbed storage has been developed using the following assumptions: temperature gradients within each rock were neglected, uniform flow distribution of air through the rockbed, rockbed storage has been divided into five isothermal sections 0.2 m long each to simulate thermal behaviour of the rockbed with satisfactory accuracy, infinite NTU model is used, no axial heat loss, no heat is stored at the beginning of a day, all collected heat by BIPV/T system (Q_{heat}) is delivered to the rockbed when exiting air temperature of the PV cavity is higher than 20 °C. Eqs. (32)–(34) have been employed in this investigation:

$$E_r = Q_{heat} \cdot n \quad (32)$$

$$\mathrm{Vol}_r = \frac{E_r}{c_r \rho_r \Delta T} \quad (33)$$

$$A_r = \frac{\mathrm{Vol}_r}{H_r} \quad (34)$$

The partial differential Eq. (35) that describes air and rock temperatures as a function of distance (x) and time (t) has been solved numerically by explicit finite difference method for each segment with a time step of 5 min.

$$-A_r \rho_r c_{pr} \frac{\partial T_r(t)}{\partial t} = \dot{m}_{air} c_{p,air} \frac{\partial T_r(x)}{\partial x} + U_r P (T_r - T_{amb}) \quad (35)$$

The rate of heat supplied by the rockbed to the zone (Q_{supply}) to cover a heating load of the zone, when air enters from the bottom and leaves from the top of the rockbed storage is given by Eq. (36):

$$Q_{supply} = \dot{m}_{air} \cdot c_{p,air} \cdot (T_{r,top} - T_{inlet}) \quad (36)$$

where T_{inlet} is equal to zone air temperature. Rockbed design data are summarized in Appendix A.

3. Experimental setup

Experimental verification of Configuration 1 model has been performed with data collected by various instruments installed at the Concordia solar house [9]. Wind speed and direction have been measured by Campbell Scientific Inc. 05103 wind monitor. Pyranometer, type LI-COR 200, has been used to monitor incident solar radiation. The PV panel surface temperatures have been measured by T-type thermocouples installed in two columns on each PV panel and properly shielded to avoid the impact of the solar radiation. Ambient temperature has been also measured by solar-shielded thermocouple. The experimental setup is presented in Fig. 5. An Agilent data acquisition and control system was utilized with VEPro software for data collection and for control [19]. The fan was operated at maximum speed and controlled to switch on when sensed incident solar radiation exceeded 10 W/m^2 at 30° slope, respectively. The air speed in the BIPV/T system was measured at five positions by TSI Velocity Meter Model 8386A with ±3% accuracy. The average value was taken as an input to the simulations. Unless stated otherwise, simulations have been done with maximum outdoor temperature of 25 °C, wind speed of 3.0 m/s and solar irradiation of 915 W/m^2.

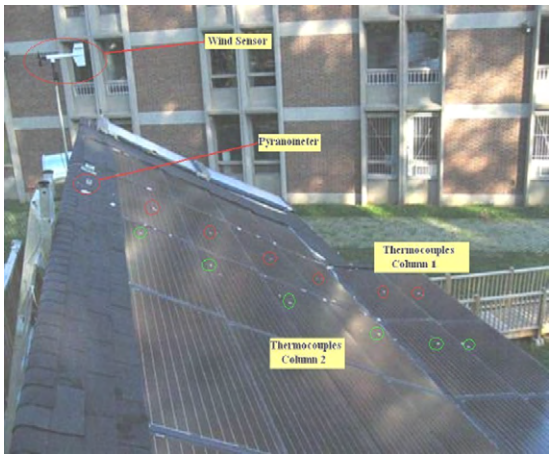

Fig. 5. Photo of solar house test facility.

In the mechanical room of the solar house, a custom made three-row AWHE with effectiveness of 0.8 has been installed. T-type thermocouples have been used for temperature measurements and have been attached at the inlet and outlet of the AWHE, both water and air side. A F-1000 Polard electronic flow meter with ±2% accuracy was mounted at the water outlet of the AWHE.

4. Results and discussion

Air temperature at the outlet of Configuration 1 air cavity is influenced by solar irradiation, cavity depth and air velocity in the cavity. The results are shown in Figs. 6 and 7. As expected, with higher levels of solar irradiation the exiting air temperature from the BIPV/T system is increased as more solar energy is available to be converted into heat. As expected, higher flow rates lead to higher rates of recovered heat and higher thermal efficiencies. Furthermore, temperature of the PV panels is decreased leading to higher electrical efficiency. However the outlet air temperatures fall as flow is increased. Thus, proper fan control strategies should be employed to ensure maximum of total energy produced—both thermal and electrical while taking into account the different values of thermal and electrical energy. Obtained results for air outlet temperature of the BIPV/T cavity as a function of solar radiation and air speed could be used for developing fan control strategies to achieve desired air outlet temperature that is selected based on desired usage. Fig. 8 shows heat removal factor (F_R) dependence on air velocity in the cavity and cavity depth of Configuration 3. As the air speed increases in the cavity, F_R also increases. This is explained by the fact that higher air velocities lead to lower air temperature rise through the air cavity. Consequently, the average PV surface temperature is decreased leading to lower heat losses and increase

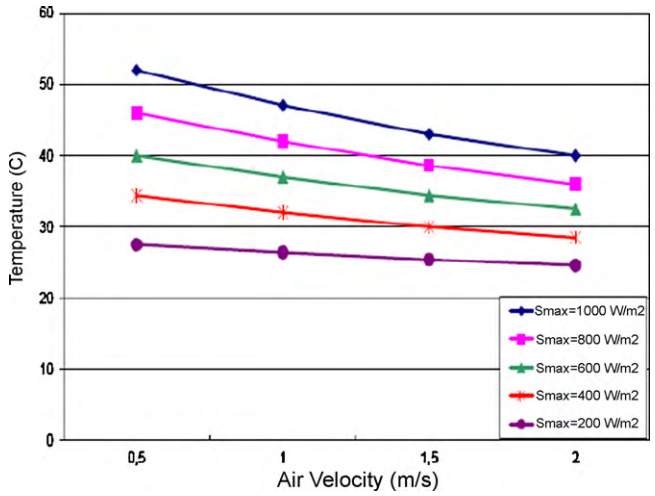

Fig. 6. Simulation results of air outlet temperature increase vs. solar radiation and varying air speeds in PV cavity of Configuration 1.

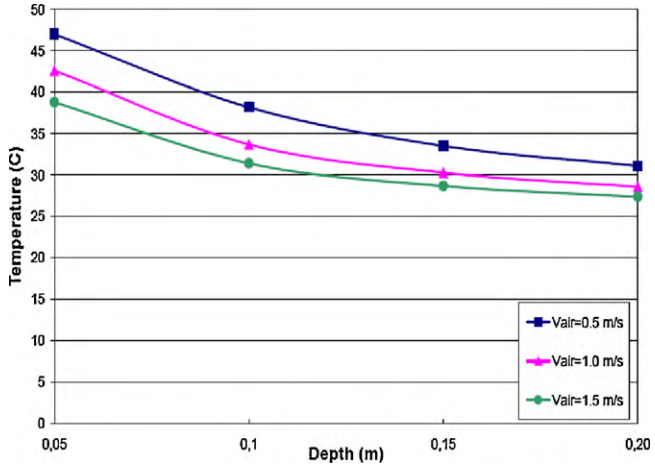

Fig. 7. Simulation air outlet temperature increase vs. PV cavity depth and varying air speeds in PV cavity of Configuration 1.

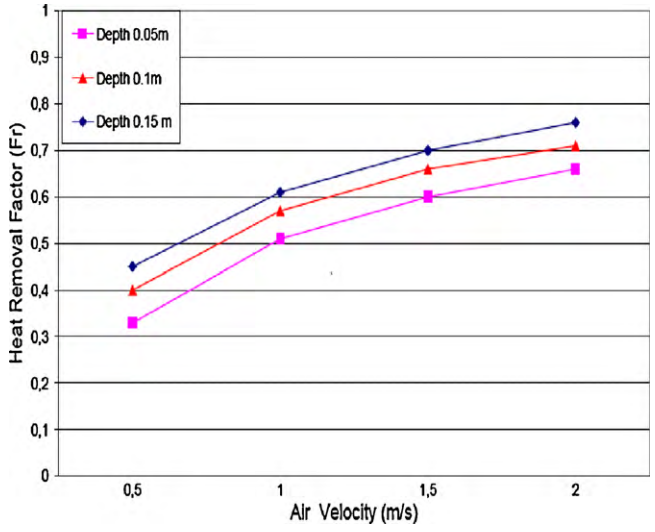

Fig. 8. Heat removal factor as a function of air speed in air cavity and depth of Configuration 3.

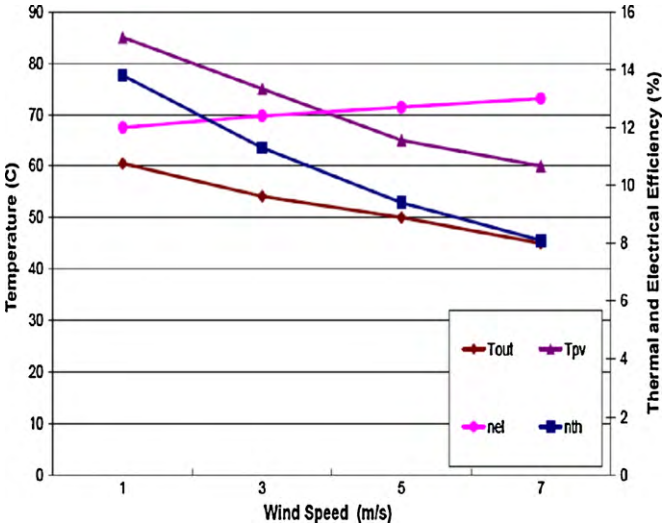

Fig. 9. Simulation results with varying wind speed of Configuration 1; $S_{max} = 1000\,W/m^2$, $V_{air} = 0.5\,m/s$, $T_{o,max} = 25\,^{\circ}C$.

in the useful energy gain and F_R. The same result is obtained with the increase of the air cavity depth as more air is transported to remove heat. Besides selecting appropriate cavity depth based on desired air temperature to be achieved, other considerations must be taken into account. If the PV cavity depth is too small, pressure drops can be too high and fan energy consumption is increased.

The PV surface and air outlet temperatures along with both thermal and electrical efficiencies of Configuration 1 as a function of wind speed are shown in Fig. 9. With increasing wind speed, the outdoor CHTC increases, resulting in increased top heat losses to the outdoor environment. Consequently, PV surface and air outlet temperatures are decreased resulting in increased electrical efficiency and decreased thermal efficiency, respectively. When wind speed from is increased from 1 m/s to 7 m/s over 4.8 m long roof, the PV panel temperature drops by about 25 °C and outlet air temperature drops by 15 °C. For the same wind speed range, electrical efficiency increases from 12% to 13% and thermal efficiency decreases from 14% to 8%. It can be concluded that wind speed has a strong impact on energy performance of the BIPV/T system and should be properly taken into consideration for analysis. Exterior CHTC found in literature have been assumed to be constant for various wind speeds, introducing some error in analysis [4]. Moreover, wind behaviour at the ground level is greatly influenced by terrain topography, surface roughness and height above the ground. Therefore, use of average daily wind speed obtained from a meteorological station usually located at the airports in analysis could also be a source of error. This is explained by the fact that wind anemometers are placed at the standard height of 10 m above the ground at locations that provide an unobstructed wind approach over the ground of similar roughness. In contrast, in urban areas, heights and arrangements of the buildings create a topography that is significantly different than that around the airports. Therefore, some corrections should be made to properly predict the wind velocity with respect to various surface roughness and height above the ground. The following power law correlation with appropriate exponents given by Eq. (37) has been found to predict the wind speed with acceptable accuracy [20]:

$$\frac{V_Z}{V_g} = \left[\frac{Z}{Z_g}\right]^{\Omega} \tag{37}$$

where V_g (m/s)is the mean gradient wind speed that corresponds to the free stream velocity at the edge of the boundary layer, Z_g (m) is the gradient height above the ground at which ground roughness

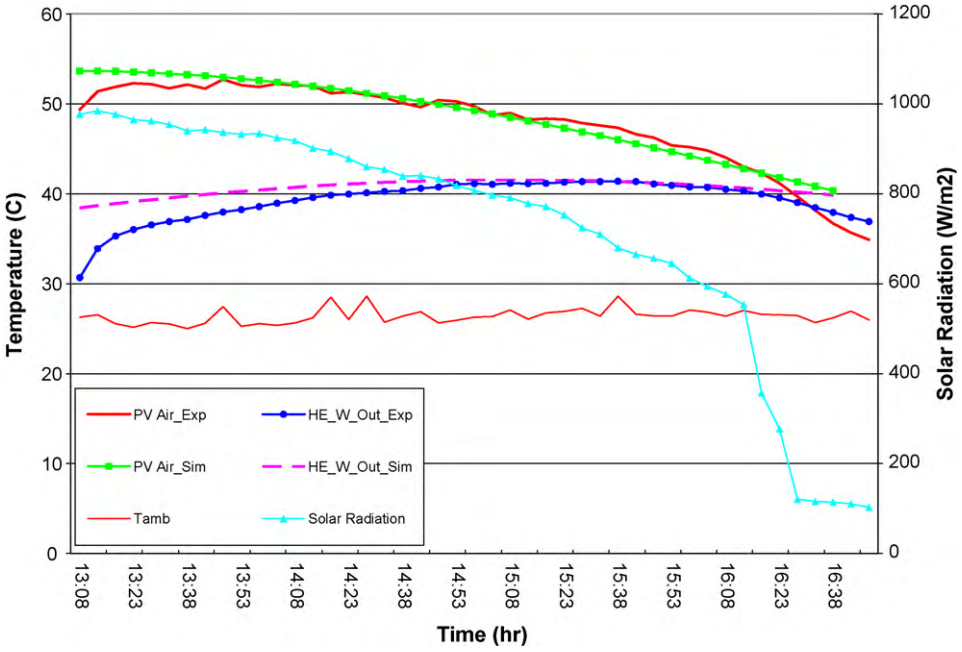

Fig. 10. Experimental and simulation results of water temperature at outlet of AWHE coupled with Configuration 1; S_{max} = 985 W/m^2, V_{air} = 0.4 m/s, V_{wind} = 2.8 m/s, $T_{o,max}$ = 26 °C (September 8th, 2006).

has no longer effect, V_z (m/s) is wind speed at any height Z (m) above the ground and Ω is the mean speed exponent that varies from 0.1 for open sea or ice to 0.4 for city centers.

Simulation and experimental data of water temperature at the outlet of the AWHE over time after interaction with Configuration 1 are presented in Fig. 10. The air speed was measured to be 0.47 m/s at the inlet of the AWHE and a water flow rate of 0.1 L/s was measured on the tank side. Incident solar radiation was 985 W/m^2 and air temperature at the top of the BIPV/T manifold was 53 °C. Data were collected on September 8th, 2006 between 13:00 and 16:40 h. It can be concluded that maximum air temperature at the outlet of the unglazed BIPV/T roof is 53 °C at 13:30 and drops afterwards as the sun goes down. Simulation results are in good agreement with experimental results; maximum water temperature of 41 °C is obtained at 15:40. Although for DHW requirements a temperature of 55–60 °C is required, significant energy savings in auxiliary heating are achieved as less energy is needed to heat the water.

Thermal energy interaction of Configurations 2 and 3 with AWHE is depicted in Fig. 11. While water temperature of 42 °C at the outlet of the AWHE could be obtained for Configuration 2, a temperature of 55 °C is obtained for Configuration 3. For practical purposes it is interesting to observe how much time is needed for heating the water in the water tank by recovered heat from all three configurations. The initial temperature of the water in the tank was set to 12 °C. Simulation results are presented in Fig. 12. It takes approximately 2 h and 50 min to heat 151 l of water from initial temperature of 12 °C to 40 °C for Configuration 1. For the same length of time, temperature of the water in the water tank is raised up to 42 °C and 55 °C by recovered heat obtained from Configuration 2 and 3 BIPV/T systems, respectively. Vertically added SAC, has not yielded any significant increase in recovered heat because the solar altitude is high in summer and thus a low amount of solar radiation is incident on a vertical surface.

Simulations of recovered heat by Configuration 2 and supplied to the thermal rockbed storage and from the rockbed to a zone have been performed. A design day in March with average wind speed of 2.2 m/s and mean ambient temperature of −2 °C has been

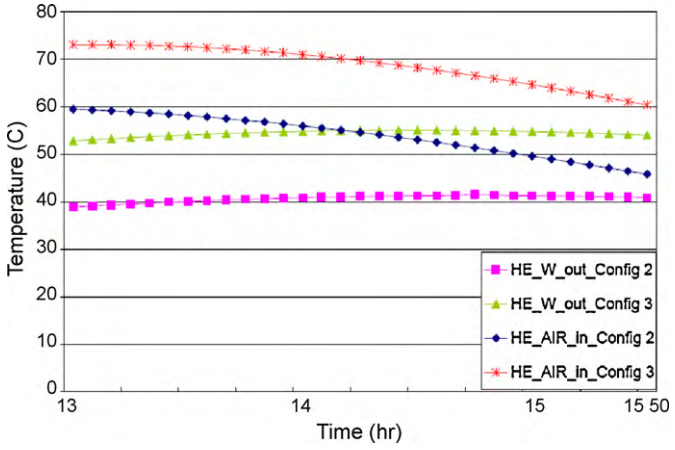

Fig. 11. Simulation results of water temperature at outlet of AHWE coupled with Configurations 2 and 3; S_{max} = 900 W/m^2, V_{air} = 0.4 m/s, V_{wind} = 2.8 m/s, $T_{o,max}$ = 26 °C.

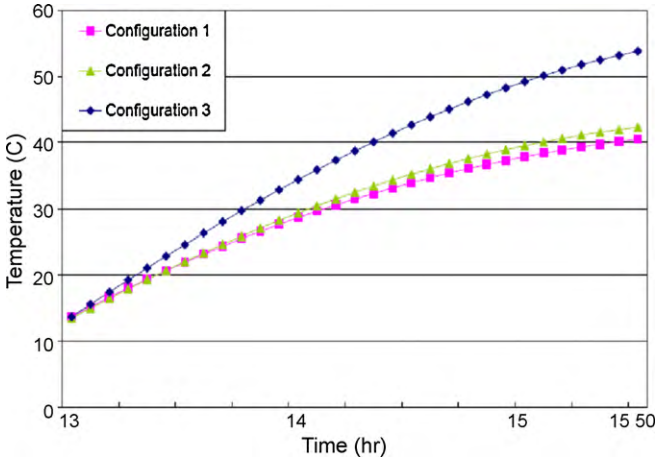

Fig. 12. Simulated water temperature distribution in DHW water tank with recovered heat obtained from Configurations 1, 2 and 3.

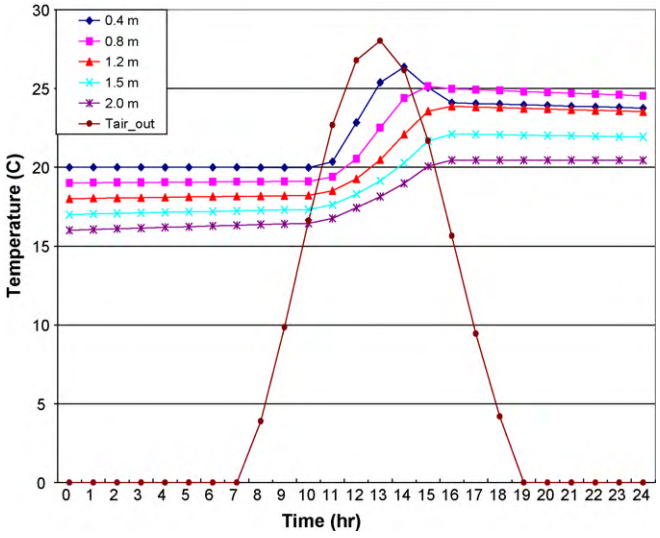

Fig. 13. Temperature distribution in rockbed storage coupled with Configuration 2.

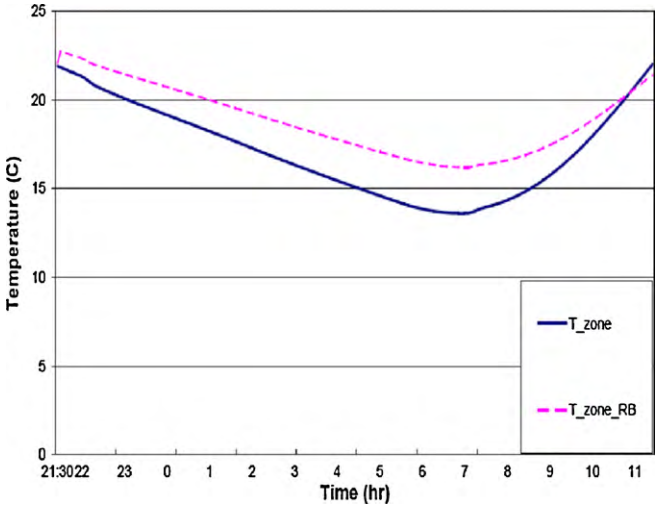

Fig. 15. Air temperature in zone before and after heat supply from rockbed coupled with Configuration 2.

selected for investigation. The air speed in the air cavity of Configuration 2 has been set equal to 1.0 m/s. Fig. 13 shows temperature distribution in the rockbed thermal storage over a 24-h period with constant air flow rate in the PV cavity (when solar radiation is received). The rockbed temperature at the top starts to increase at about 11:00 h, rises to 26 °C at 14:00 and decreases to about 24 °C at 16:00. After 15:00, the rockbed temperature at depth of 0.8 m is lower than that at a depth of 0.4 m. This phenomenon is explained by the fact that heat is being collected at decreasing temperatures, cooling the upper zones in the rockbed storage and pushing the peak temperature downward. After 16:00 when the fan is turned off, temperatures of the top layers in the rockbed are slightly decreasing and bottom layer temperatures are slightly increasing.

Fig. 14 shows comparison of the zone heat load before and after heat supply from the rockbed storage coupled with Configuration 2. A reduction in heating load is found to be approximately 48.5%. Fig. 15 shows zone air temperature profiles before and after heat supply from the rockbed storage coupled with Configuration 2. Increase in zone temperature of 2.5 °C is observed.

To properly address energy potential of contrasted BIPV/T configurations, both thermal and electrical energy performance over a typical summer and winter day along with maximum PV panel and air outlet temperatures are presented in Figs. 16 and 17.

In summer, Configurations 1 and 2 have higher electrical efficiency than Configuration 3 and produce about 50% more electrical energy. This is explained by the fact that glazing cover of Configuration 3 reduces solar input compared to the other two Configurations. Moreover, significantly high PV surface temperature of Configuration 3 resulted not only in reduced electrical efficiency and electrical energy production but may also jeopardize structural stability and reduce operational life time of PV panels as most PV manufacturers recommend keeping PV surface temperature lower than 75 °C. In contrast, recovered heat by Configuration 3 is about 75% higher than that of Configurations 1 and 2. Moreover, its air outlet temperature is increased by about 45% more than that of the other two configurations, making it suitable for heating applications, e.g. DHW preparation. Vertically added SAC to Configuration 1 has yielded some increase in thermal energy and air outlet temperature. Thermal efficiency of Configuration 2 is lower than that of Configuration 1 due to increased available collection area.

In winter Configurations 1 and 2 produce significantly more electricity than Configuration 3. In contrast, thermal efficiency and generated thermal energy of Configuration 3 are significantly higher than those of Configurations 1 and 2. Outlet air of BIPV/T

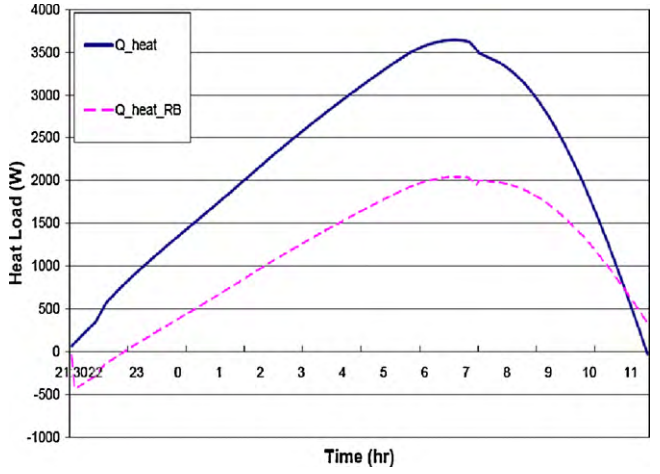

Fig. 14. Heat load in zone before and after heat supply from rockbed coupled with Configuration 2.

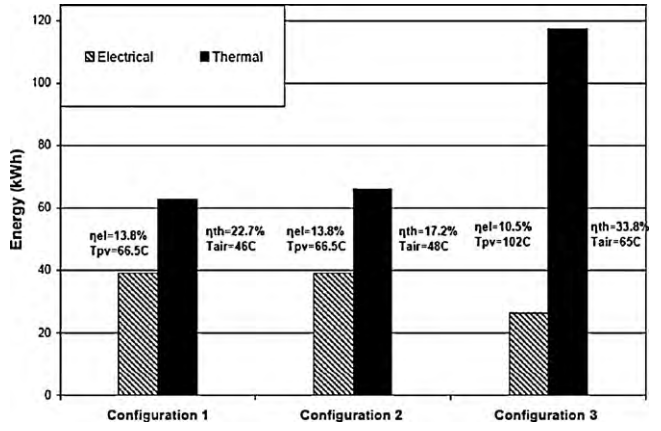

Fig. 16. Typical summer BIPV/T energy production for the three configurations (electrical and thermal efficiencies indicated, max. PV panel and air outlet temperature of Configurations 1, 2 and 3 on July 17th with S_{max} = 912 W/m^2, V_{air} = 1 m/s, V_{wind} = 3 m/s and $T_{o,max}$ = 27 °C).

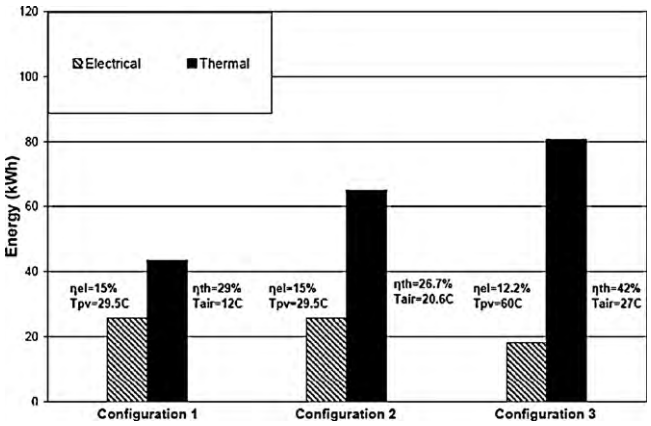

Fig. 17. Typical winter BIPV/T energy production for the three configurations (electrical and thermal efficiencies are indicated, max. PV panel and air outlet temperature of Configurations 1, 2 and 3 on February 16th; S_{max} = 716 W/m^2, V_{air} = 1 m/s, V_{wind} = 3 m/s, $T_{o,max}$ = −15.6 °C).

configurations may be used as a preheated air in HVAC system. For Configuration 2, harvested heat is up to 50% higher than that of Configuration 1. Moreover, by vertically adding 1.5 m long SAC to Configuration 1, an air temperature increase of about 8.5 °C has been achieved.

Figs. 18 and 19 compare PV power output for the three configurations on typical summer and winter days, respectively. Both graphs follow the sun movement and are strongly influenced by intensity of solar irradiation. For the same PV area, Configuration 3 generates 25% less electricity than that of Configurations 1 or 2 for both weather scenarios due to reduced solar input transmission through glass cover and higher PV surface temperature (exceeds 100 °C). About 12.5% more power is generated by all configurations on a typical summer day as compared to that of a typical winter day.

Further work is planned to compare the performance of different BIPV/T systems using lifecycle analysis and the different values of electrical and thermal energy produced. Normally, electricity is assumed to be about 3–4 times as valuable as thermal energy. The thermal energy recovered from BIPV/T systems such as the ones considered in this study is about 2–4 times as much as the electricity produced. Important factors in a comparative economic analysis are the assumed lifetimes of the systems, as well as the possibility of using different time-of-day rates for electricity.

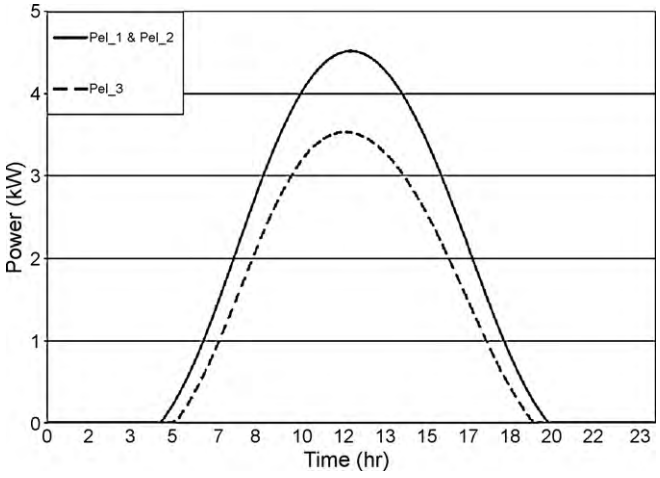

Fig. 18. PV Power outputs of Configurations 1,2 and 3 on July 17th, S_{max} = 912 W/m^2, V_{air} = 1 m/s, V_{wind} = 3 m/s, $T_{o,max}$ = 27 °C.

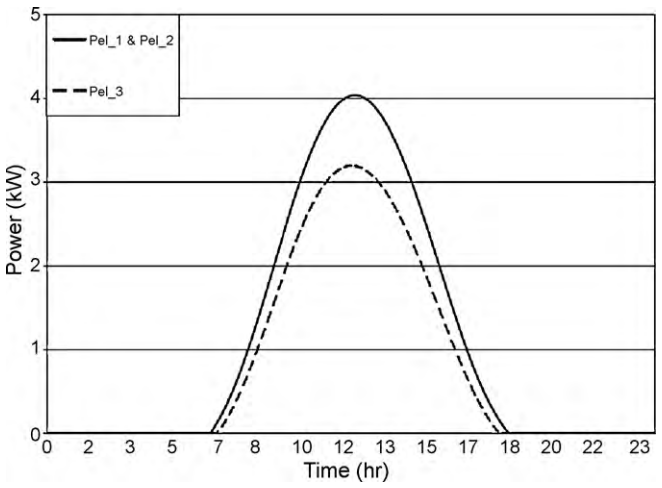

Fig. 19. PV Power outputs of Configurations 1, 2 and 3 on February 16th, S_{max} = 716 W/m^2, V_{air} = 1 m/s, V_{wind} = 3 m/s, $T_{o,max}$ = −15.6 °C.

5. Conclusions

This paper compared three different open loop air-based building-integrated photovoltaic/thermal systems coupled with roof, their integration with forced air heating systems and utilization of the recovered heat to increase thermal efficiency. The following three BIPV/T systems have been considered in detail:

- Unglazed BIPV/T roof (Configuration 1).
- Unglazed BIPV/T roof connected to a glazed solar air collector (Configuration 2).
- Glazed BIPV/T roof (Configuration 3).

Mathematical models have been developed for all three systems and have been compared on a relative basis.

Air flow in the BIPV/T cavity should be selected as a function of desired outlet temperatures and fan energy consumption. Cavity depths, air velocity in the air cavity and wind speed have significant affect on the unglazed BIPV/T system energy performance. Development of efficient fan control strategies is an important step in designing effective BIPV/T systems. Simulation results for exiting air temperatures of the BIPV/T cavity as a function of incident solar radiation levels and air speed in the cavity may be used for developing fan control strategies to achieve desired air outlet temperature as a function of end use. Configurations 2 and 3 may be utilized to significantly increase thermal efficiency and air outlet temperature. In contrast, Configuration 3 significantly reduces electricity production and may lead to excessively high temperatures of the PV panels and is thus not recommended unless means for removing the heat are employed such as cooling fins and higher flow rates. The unglazed BIPV/T system linked to a short vertical solar air collector is suitable for a connection with a rockbed thermal storage due to the higher thermal energy production in winter. Finally, the air in an open-loop BIPV/T system may be used as preheated fresh air after being filtered.

Acknowledgements

Financial support of this work was provided by NSERC through the Solar Buildings Research Network and by Natural Resources Canada through the Innovative Research Initiative and the Technology and Innovation Program as part of the Climate Change Plan for Canada.

Appendix A.

Rockbed design data

Parameter	Value
Rock diameter (m)	20×10^{-3}
Rock porosity	0.4
Rock density (kg/m^3)	1533
Rock conductivity (W/m K)	0.125
Rock specific heat (J/kg K)	880
Change in rockbed temperature (°C)	30
Days of required heat storage	1
Rockbed height (m)	2
Rockbed volume (m^3)	6.6
U value of rockbed (W/m^2 K)	1.8
Initial section temperature 1–5 (°C)	20–16, step 1

References

[1] Y. Wang, W. Tian, J. Ren, L. Zhu, O. Wang, Influence of a building's integrated-photovoltaics on heating and cooling loads, Applied Energy 83 (2006) 989–1003.

[2] M. Bazilian, F. Leenders, B. Van Der Ree, D. Prasad, Photovoltaic cogeneration in the build environment, Solar Energy Vol.71 (1) (2001) 57–69.

[3] L. Liao, A. Athienitis, L. Candanedo, K.W. Park, Numerical and experimental study of heat transfer in a BIPV-thermal system, Journal of Solar Energy Engineering 129 (2007) 423–430.

[4] R. Charron, A. Athienitis, Optimization of the performance of double-facades with integrated photovoltaic panels and motorized blinds, Solar Energy 80 (2006) 482–491.

[5] A. Guiavarch, B. Peuportier, Photovoltaic collector efficiency according to their integration in buildings, Solar Energy 80 (2006) 65–77.

[6] J. Ji, J. Han, T. Chow, H. Yi, J. Lu, W. He, W. Sun, Effect of fluid flow and parking factor on energy performance of a wall-mounted hybrid photovoltaic/water-heating collector system, Energy and Buildings 38 (2006) 1380–1387.

[7] M. Bakker, H. Zondag, M. Elswijk, K. Strootman, M. Jong, Performance and costs of a roof-sized PV/thermal array combined with a ground coupled heat pump, Solar Energy 78 (2005) 331–339.

[8] J.A. Candanedo, B. O'Neill, S. Pantic, A. Athienitis, Studies of control strategies for the Concordia solar house, in: Proceedings of the 2nd Canadian Solar Buildings Conference, Calgary, Canada, 2007.

[9] M. Pasini, A.K. Athienitis, Systems design of the canadian solar decathlon house, ASHRAE Transactions 112 (Pt. 2) (2006) 308–319.

[10] Y. Chen, A.K. Athienitis, K.E. Galal, Y. Poissant, Design and simulation for a solar house with building integrated photovoltaic-thermal system and thermal storage, in: Proceedings of the ISES Solar World Congress, vol. I, Beijing, China, 2007, pp. 327–332.

[11] MathCAD Professional 2001i, Mathsoft Engineering & Education Inc., Cambridge, MA, USA, 2001.

[12] M. Mottillo, I. Beausoleil-Morrison, L. Couture, Y. Poissant, A Comparison and Validation of 2 Photovoltaic Models, Canmet Energy, NRCAN, Canada, Visited: December 15th, http://canmetenergy-canmetenergie.nrcan-rncan.gc.ca, 2009.

[13] J. Duffie, W. Beckman, Solar Engineering of Thermal Processes, 2nd ed., John Wiley & Sons, New York, USA, 1980.

[14] F. Incropera, D. DeWitt, Fundamentals of Heat and Mass transfer, 2nd edition, John Wiley & Sons, New York, USA, 1985.

[15] K. Ong, Thermal performance of solar air heaters: mathematical model and solution procedure, Solar Energy 55 (2) (1995) 93–109.

[16] V. Gnielinski, Forced Convection in Ducts, Hemisphere Publishing Corporation, 1983.

[17] T.M. McClellan, C.O. Pedersen, Investigation of outside heat balance models for use in a heat balance cooling load calculation procedure, ASHRAE Transactions 103 (Pt. 2) (1997).

[18] A. Athienitis, M. Santamouris, Thermal Analysis and Design of Passive Solar Buildings, James & James Ltd., London, UK, 2002.

[19] Agilent VEE Pro 8.0, Agilent Technologies Inc., Santa Clara, CA, USA, 2006.

[20] N. Hutcheon, G. Handegord, Building Science for a Cold Climate, National Research Council of Canada, 1995.